Inference on Hippocampal Connectivity Using Multi-Trial Count-Valued Time Series

Adam Kiehl

5/11/22

This thesis was submitted to the Colorado State University Honors Program office in May 2022 in partial fulfilment of Adam Kiehl's Honors graduation requirements. It was also submitted to the Data Science Capstone course in partial fulfilment of his degree requirements. An individual contribution report (indicated by the formal proposal) was not included since research was ultimately done independently, contrary to the proposed plan. Dr. Aaron Nielsen, Gray Stanton, and Dr. Emily King served as advisors to the project. It was reviewed by Dr. Don Mykles of the University Honors Program.

Abstract

Inference on neural connectivity is of great interest to researchers in the fields of medicine, engineering, psychology, and more. As a demonstration of the feasibility of using longitudinal generalized linear models to this purpose, inference was performed in this analysis on the brain of a rat. Multi-trial count-valued spike train data collected by researchers at the University of Southern California [14] were used to explore the connections between two regions of the rat's hippocampus as well as within-region connections. An array of models from the GLAR, INGARCH, and GLARMA frameworks were trained and validated, and neural connectivity maps were developed based on the results. All frameworks exhibited similar predictive capabilities, so neural inference was ultimately not overly sensitive to model choice.

1 Introduction

The human brain is widely considered one of the most complex systems in the known universe. It is estimated to contain 86 billion neurons that communicate with each other through electrical impulses that travel along intricate circuit-like pathways in a fraction of a second. For the purposes of research and medicine, understanding the specifics of neural connectivity is of great interest to science. Knowledge concerning this connectivity has implications for the fields of brain surgery, neural engineering, psychology, and many more.

Several methods have been developed for measuring neural activity. The most common and least invasive procedure is called functional magnetic resonance imaging (fMRI), which infers neural activity based on oxygenated blood flow tracked with a large imaging machine and injected dye [7]. Superior resolution both in spatial and temporal terms can be achieved by measuring the brain's electrical impulses more directly. Electroencephalography (EEG) and electrocorticography (ECoG) achieve this through an array of electrodes placed on and under the scalp, respectively [7]. More invasive methods can produce even better resolution. Electrodes embedded in the brain itself can measure local electrical pulses known as action potentials that indicate activity in a nearby neuron [1]. The output, known as a spike train, provides timestamps of each recorded action potential in the locality of the electrode.

A study by researchers at the University of Southern California (USC) [14] attempted to utilize such spike trains to perform inference on neural connectivity in the hippocampus of a rat with the aim of laying the groundwork for a "cognitive prosthesis" that could replace damaged areas of the brain. Their research focused on the temporoammonic pathway (Figure 1), which connects two regions (CA3 and CA1) of the hippocampus and has been linked with facilitating the encoding of spatial memory [14]. A rat was observed as it repeatedly participated in a three-stage task involving levers and a button, that would result in a reinforcement reward if correctly performed. Spike train data were recorded in the two hippocampal regions of interest. They then utilized a complex multi-input, multi-output (MIMO) sparse generalized Laguerre-Volterra model (SGLVM) to mathematically simulate the pathway between CA3 and CA1. Their research was able to thoroughly describe linkages between the regions and was able to identify sections of the spike train data that appeared repetitiously in conjunction with moments in the task, thus effectively translating between neural activity and spatial memory formation.

This analysis will explore the possibility of using generic count-valued time series models, rather than custom SVGLM [14], to identify specific linkages along the temporoammonic pathway. Based on the generalized linear model (GLM) framework, the models of interest here are simpler and easier to implement than the aforementioned SGLVM while not providing as high a level of clarity. A similar analytical structure was implemented based on the connectivity between CA3 and CA1 and was extended by studying within-region connectivity as well.

2   Data

The data collected by the USC researchers [14] were repurposed for this analysis. The data were collected in approximately hour-long sessions over the course of several days. A microwire multi-electrode array (MEA) was surgically implanted into the hippocampus of a rat with 8 electrodes each in CA1 and CA3. It was not assumed that each electrode was only activated by a single neuron since signals were contaminated by other nearby signals; therefore, a spike-sorting approach was utilized to discriminate between different signal sources [11]. In
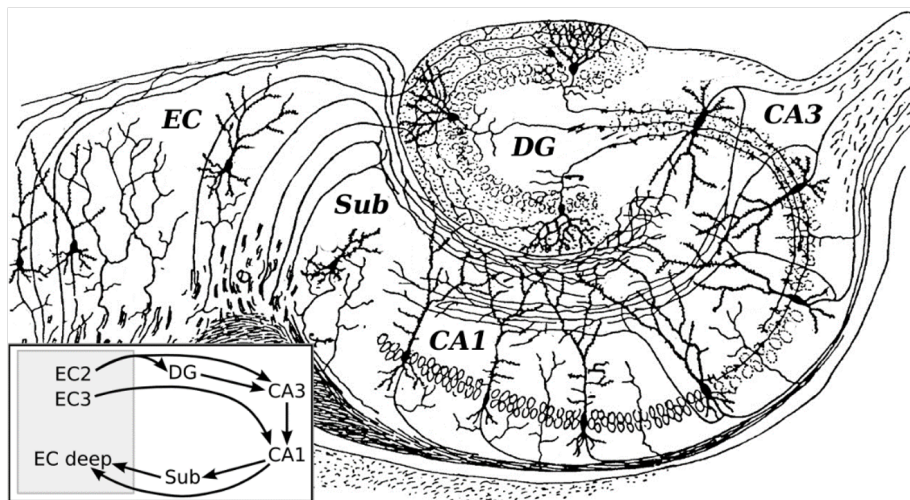
Figure 1: The linkage between the CA3 and CA1 regions of the hippocampus form the temporoammonic pathway, which has been identified as being important in facilitating the encoding of spatial memory [14].

total, 15 neurons (CA1.1,..., CA1.15) in CA1 and 21 (CA3.1,..., CA3.21) in CA3 were observed.

Action potential measurements were made continuously as the rat repeatedly underwent a three-stage task with each repetition being recorded as a single trial. The stages were 1) a "sample response" phase in which the rat was presented a lever to press, 2) a "delay phase" in which the rat had to poke a button with its nose while waiting for the next phase, and 3) a "non-match" phase in which the rat was presented with two levers and had to select the lever opposite the one presented at the beginning of the trial. A single trial lasted 31 seconds, on average. For each trial, timestamps were recorded for the beginning and end of the trial, the introduction of a reinforcement reward, and the beginning and end of the delay phase. The trial outcome (success/non-success) was also noted. For each action potential, the region and neuron were recorded along with the timestamp of the spike.

The data were binned into 0.5 second intervals to yield count-valued time series for each neuron (Figure 2). Trials where data were missing for one or more neurons were excluded and only trials from the first day of testing were used since measurements were mechanically limited by electrode drift, which describes how the instruments can migrate over time, making cross-day comparisons assumptive [11]. 40 of the 46 complete trials were used as a training set and the remaining six were held out as a testing set.
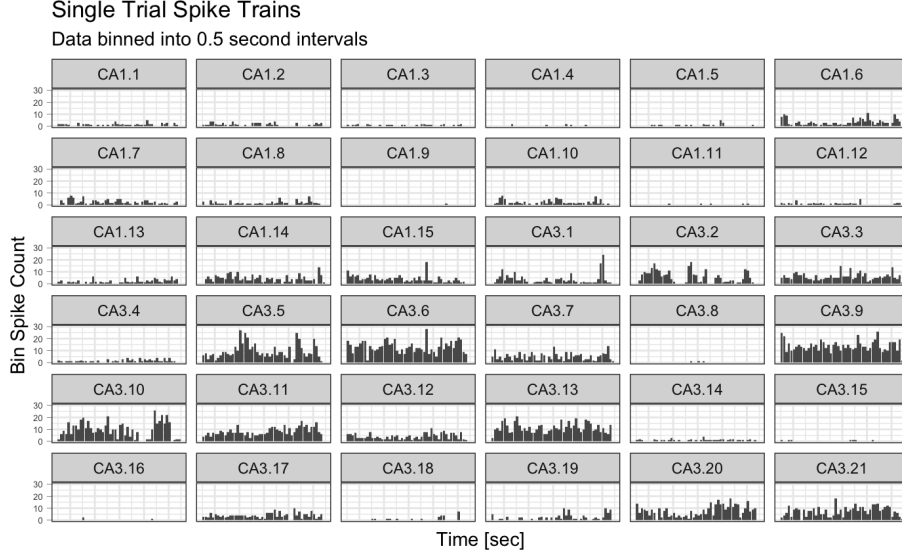
Figure 2: Spike train data for every observed neuron for the length of one trial. The data were binned along 0.5 second intervals and only trials with complete data were used.

3 Methods

In this analysis, multi-input, single-output (MISO) models were used to relate the time series of individual output neurons in CA1 with the time series of selected predictor neurons of interest. While inter-region connectivity was the primary focus of the USC researchers [14], this demonstration allowed for consideration of within-region connectivity as well. For each model specification, a strictly inter-region and a strictly within-region version was fit. No evidence was found that neural activity diminished over the course of the testing period, as measured in spikes per second. However, trial number was also included as a predictor in all models to formally account for any such trend.

Several different model frameworks were implemented since no standard modeling method has been established for count-valued time series [5]. All models used were derived from the GLM framework. Models of this class assume a probability distribution for the response variable and model the parameterization of that distribution (the random component) as a linear combination of covariates (the systematic component), typically through a link function [9]. The chosen model frameworks also incorporated longitudinal modifications to account for modeling with time series data. Lagged values of the response neuron, and sometimes a lagged conditional mean, were incorporated into the systematic component to account for dependence between observations. For all model specifications below, consider a response time series $\{Y_t : t \in \mathbb{N}\}$, a matrix of covari-

4

ate time series $\mathbf{X}_t = (X_{t,1}, ..., X_{t,r})^T$, a joint process $F_t = \{Y_t, \lambda_t, \mathbf{X}_{t+1} : t \in \mathbb{N}\}$, and a log-link transformation $\nu_t = \log(\theta_t)$ for some distributional parameter θ.

The first and simplest model used in this analysis was the generalized linear autoregressive (GLAR) model. It is indexed by p, the number of lagged values of the response time series to include in the model as predictors [5].

$$\nu_t = \beta_0 + \sum_{i=1}^{p} \beta_j \log(Y_{t-i} + 1) + \boldsymbol{\eta^T X_t}$$

An intercept (β_0) and coefficients for each lag (β_j) and for each covariate (η) are estimated via maximum likelihood. For this analysis, the GLAR implementation in the `tscount` CRAN package [8] was used. The second model used was the integer generalized autoregressive conditional heteroscedastic (INGARCH) model framework, which extends the GLAR framework slightly to include regression on a lagged conditional mean, indexed by an additional value, q [5].

$$\nu_t = \beta_0 + \sum_{i=1}^{p} \beta_j \log(Y_{t-i} + 1) + \alpha \nu_{t-q} + \boldsymbol{\eta}^T \boldsymbol{X}_t$$

Here, an additional coefficient (α) is estimated for the lagged conditional mean. This model is also implemented by the `tscount` package [8]. Both above models are considered observation-driven because the latent state is defined as a deterministic function of past observations. This is opposed to parameter-driven models where the state is defined stochastically [4]. The final framework used, the generalized linear autoregressive moving average (GLARMA) model, is parameter-driven but also includes a deterministic component e_t [5].

$$e_t = \frac{Y_t - \mu_t}{\sigma_t}$$

$$Z_t = \sum_{i=1}^{p} \phi_i Z_{t-i} + \sigma_t e_{t-1} + \theta e_{t-1-q}$$

$$\nu_t = O_t + Z_t + \boldsymbol{\eta^T X_t}$$

This method estimates an intercept (O_t), coefficients for each lag (ϕ_i), and a coefficient for the lagged conditional mean (θ). An implementation of this model in the `glarma` CRAN package [6] was used.

The standard assumed response distribution for integer GLMs is the Poisson distribution $Y_t | F_{t-1} \sim \text{Poisson}(\lambda_t)$ with rate parameter λ_t where $\mu_t = \lambda_t$.

$$P(Y_t = y | F_{t-1}) = \frac{\lambda_t^y e^{-\lambda_t}}{y!}, \quad y = 0, 1, 2, ...$$

This distribution was used for all models. However, some evidence of overdispersion was found in the vast majority of models, as calculated by the `tscount` package [8]. This finding was also confirmed through diagnostic probability integral transform (PIT) diagrams. This occurs when sample variance is greater

than expected by the model. The negative binomial distribution $Y_t|F_{t-1} \sim$ NegBinom(λ_t, ϕ_t) is also frequently used to describe count-valued data but is better equipped to handle overdispersion.

$$P(Y_t = y|F_{t-1}) = \frac{\Gamma(\phi + y)}{\Gamma(y+1)\Gamma(\phi)} \left(\frac{\phi}{\phi + \lambda_t}\right)^\phi \left(\frac{\lambda_t}{\phi + \lambda_t}\right)^y, \quad y = 0, 1, 2, ...$$

Therefore, all GLAR and INGARCH models were also fit using the negative binomial assumption. The `glarma` package [6] was unable to fit models using this assumption. In all, for each of the 15 output neurons in CA1, ten MISO models were fit: four GLAR models (Poisson inter-region and within-region, negative binomial inter-region and within-region), four INGARCH models (the same), and two GLARMA models (Poisson only).

A multi-stage model optimization procedure was developed for variable selection and parameter tuning. A blocked cross-validation method [13] similar to k-fold cross-validation but modified for temporal dependence was used for optimization calculations. Following this method, data were divided into time-continuous folds rather than randomly partitioned. Within each fold, training was performed on the first 80% of data and validation on the latter 20%. Mean squared error (MSE) was used for model comparison during the optimization of GLAR and GLARMA models. Due to the time complexity of forecasting with the `glarma` package [6], the Akiake information criterion (AIC) was used as a proxy for MSE during GLARMA optimization. First, full models were fit using all associated predictors (all CA3 neurons for inter-region and all but one CA1 neuron for within-region). Due to the large number of covariates available, a forward selection procedure was implemented based on the magnitude of the estimated covariate coefficients from the full model. Optimal predictor sets were recorded for each of the 150 models of interest. Those predictors were then used in a model tuning procedure that looped through reasonable values of p and q (1,...,5) for multi-index models and p for single-index models. Final models were then fit on the entire training set using the optimal predictor sets and index values and were tested against the held-out six-trial testing set.

Due to the computational complexity of the model optimization procedure used, all calculations were performed by the Summit High Performance Computing (HPC) system [10], available to researchers at the University of Colorado Boulder and Colorado State University. Batch request scripts were written to activate a constructed Conda environment and facilitate the compilation of the modeling scripts written in R. It took 1.6 hours, on average, to completely fit each variety of GLAR model for all response neurons, 7.9 hours for INGARCH, and 6.5 hours for GLARMA.

As an experimental detection of associations between neurons, an exploratory normalized cross-correlation matrix [2] was generated (Figure 3) using the `tseries` CRAN package [16]. The maximum correlation value across lags was taken to find the greatest extent of cross-neuron association during the experiment. The matrix is divided into three sections: inter-region correlations (bottom right), intra-CA1 correlations (top right), intra-CA3 correlations (bottom left).
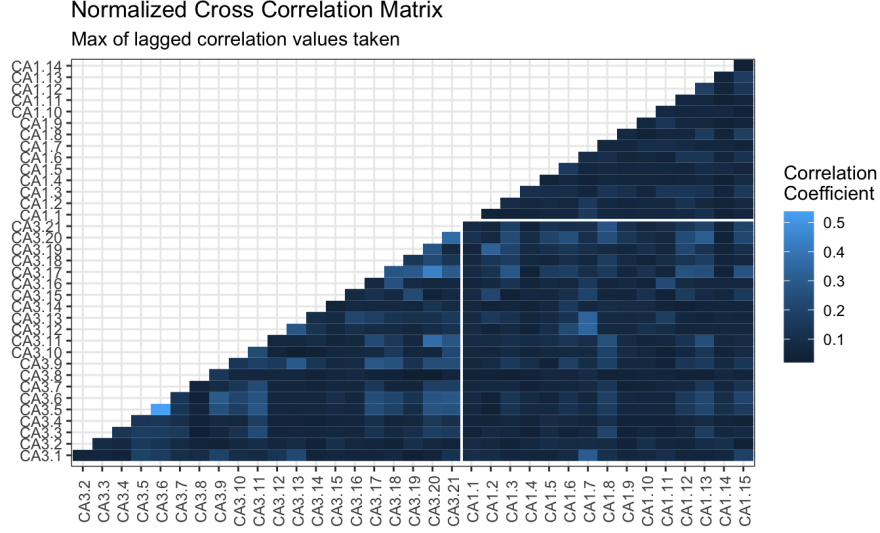
Figure 3: Normalized cross-correlation matrix for all observed neurons. The maximum correlation value across lags is shown. The matrix is divided into three sections: inter-region correlations (bottom right), intra-CA1 (top right), intra-CA3 (bottom left).

4   Results

Before results were analyzed, model diagnostic plots were examined to verify the validity of assumptions and methodologies [8]. Autocorrelation function (ACF) plots were used to test for serial autocorrelation in time. Residual plots were used to test for the homogeneity of model residuals over time and Q-Q plots were used to test for normality of said residuals. Marginal calibration plots were used to test for differences between the predicted and empirical cumulative distribution functions (CDF) of the assumed response distributions. PIT diagrams were also used to assess the appropriateness of the assumed response distribution. Only two model diagnoses revealed obvious evidence of violated assumptions. The negative binomial INGARCH within-region model for neuron CA1.4 showed evidence of underdispersion and correlation between model residuals and time. The GLARMA inter- and within-region models for neuron CA1.9 did not converge well when estimating coefficients and a clear correlation between model residuals and time was present.

From the correlation matrix (Figure 3), it is visually apparent that the CA3 input neurons have a great deal of intercorrelation while the CA1 output neurons appear to be relatively uncorrelated. Scattered notable correlations were observed in the inter-region section but they did not consistently agree with optimally selected predictor variable sets. These results suggest that predictive

accuracy will be greater for inter-region models than within-region models.
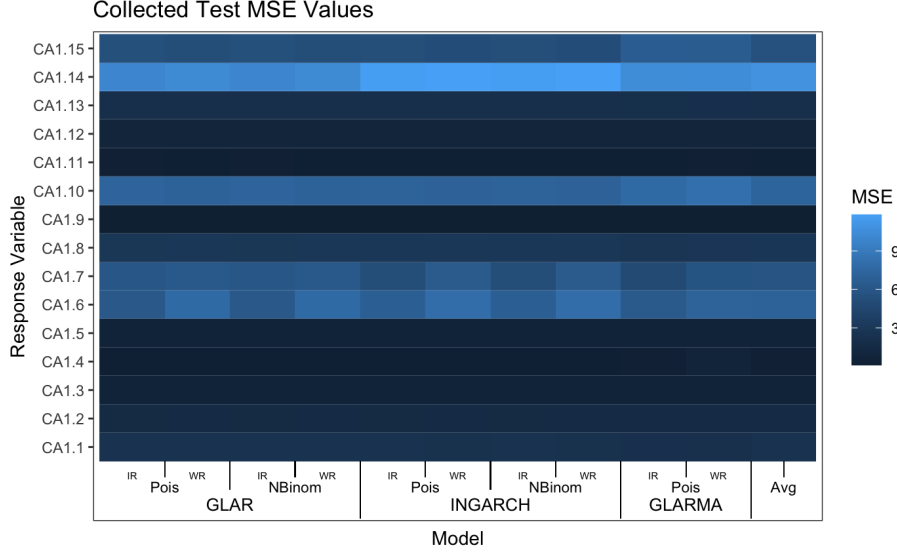

Figure 4: Test MSE values were calculated for all models using the data from the six held-out trials. Large variability in MSE was found between output neurons but not between model frameworks or region methods.

All models were compared with test MSE values calculated using the data from the six held-out test trials (Figure 4). Normalized MSE (NMSE) values (Figure 5) were also calculated using the `TSPred` CRAN package [12] to adjust MSE values relative to signal size [3].

$$\text{NMSE} = \sqrt{\frac{\sum_i (\hat{y}_i - y_i)^2}{\sum_i (y_i - \bar{y})^2}}$$

No evidence of notable differences between the predictive abilities of the GLAR, INGARCH, and GLARMA model frameworks was present. Further, corresponding models that differed only by the distributional assumption used (Poisson vs negative binomial) had nearly identical predictive capacities. Some evidence was found to suggest a difference between the predictive abilities of inter-region and within-region models. In terms of NMSE, inter-region models outperformed within-region models for almost all neurons. This finding was especially apparent for neurons CA1.6 & 9 and was supported by the exploratory correlation matrix developed (Figure 3). More so than model framework or distributional assumption, the largest source of variability in model accuracy was the output neuron of interest. To study this phenomenon, average MSE and NMSE were calculated across all models for each output neuron (Table 1). The CA1.3, 4, 5, 9, 11, & 12 neurons were particularly suitable for the models
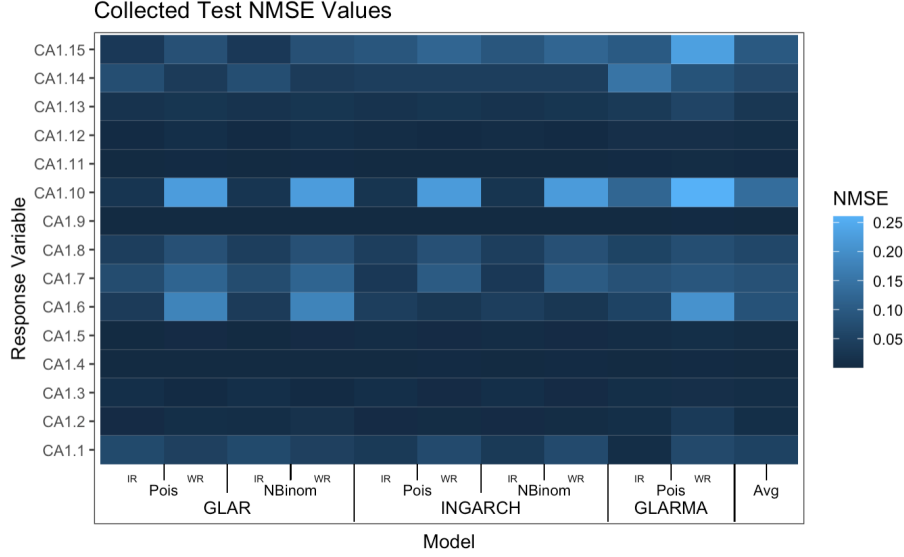
Figure 5: Test NMSE values were calculated for all models using the data from the six held-out trials. Large variability in NMSE was found between output neurons and between region methods but not between model frameworks.

used in this analysis and all had test MSE values, on average, less than one and test NMSE values, on average, less than 0.01. On the other hand, the CA1.6, 7, 10, 14, & 15 neurons all had test MSE values, on average, greater than five and test NMSE values, on average, greater that 0.05. In the domain of MISO modeling, this may imply that those neurons with highly predictive models also likely have a great degree of local neural connectivity.

Inter-neuron connectivity was primarily measured using the magnitude of estimated model coefficients as a proxy. Neural maps (Figures 6-11 found in the appendix) were developed to visualize connections. While only negligible differences in test MSE and NMSE between model frameworks were detected, each framework's estimator is slightly different and produced slightly differing coefficient estimates. Coefficient magnitudes relative to other predictor coefficients within the same model were compared across models. Between GLAR (Figures 6 & 7) and INGARCH (Figures 8 & 9) models, relative estimates and selected predictors were largely similar but differed more substantially from those produced by the GLARMA models (Figures 10 & 11). In most cases, coefficient estimates for lagged observations (β for GLAR and INGARCH and ϕ for GLARMA) were relatively large for a single lag but got progressively smaller for progressively distant lagged values. These lagged values were featured more prominently in the GLAR models, which did not include a lagged conditional mean (α for INGARCH and θ for GLARMA) to regress against. The CA1.2, 4, & 14 neurons were particularly strongly associated with their past mean in the

Neuron	MSE	NMSE
CA1.1	2.307	0.049
CA1.2	1.453	0.009
CA1.3	0.534	0.007
CA1.4	0.203	0.001
CA1.5	0.489	0.004
CA1.6	7.066	0.083
CA1.7	5.789	0.081
CA1.8	2.844	0.061
CA1.9	0.096	0.001
CA1.10	7.259	0.136
CA1.11	0.178	0.001
CA1.12	0.772	0.006
CA1.13	2.058	0.026
CA1.14	10.831	0.062
CA1.15	5.471	0.097

Table 1: MSE and NMSE values were averaged across all models for each neuron. CA1.3, 4, 5, 9, 11, & 12 exhibited notably low MSE and NMSE values. CA1.6, 7, 10, 14, & 15 exhibited notably high MSE and NMSE values.

INGARCH models. Coefficient estimates for trial number were all near-zero.

Counter to what was suggested by the exploratory correlation matrix, within-region CA1 neural connectivity (Figures 8-10) was found to be greater than inter-region connectivity as more neurons were included in the optimal within-region predictor sets. Interestingly, past lagged values were also treated as more predictive in within-region models than in inter-region models. However, this connectivity does not imply greater predictivity as the within-region models did not have superior predictive performance to the inter-region models.

5 Discussion

The estimated model coefficients were used as inferential tools to simulate neural connectivity. A coefficient estimate was thought to imply a degree of influence on an output neuron by the associated input neuron (e.g., between CA3.16 & CA1.9). Further, the magnitude of the estimate may imply a relatively strong or weak neural connection. Most neural connections were found to be of similar strength with only several standing out as being noticeably more robust (e.g., between CA1.11 & CA1.9). Such connections were, as expected based on the cross-correlation matrix calculated, found more frequently among within-region comparisons. However, the number of connections was not necessarily indicative of high predictability since inter-region models outperformed within-region models in terms of NMSE. Influence was also found between many output neurons and their own lagged time series values up to 2.5 seconds. This may be due to repetitious action potential patterns that can occur when a neuron is consis-

tently engaged throughout an entire phase of the rat's task. Trial number, also as expected, was not consequentially related to neural output activity as the same experiment was performed in each trial. Ultimately, all GLM frameworks demonstrated similarly acceptable predictive capabilities; neural inference was not sensitive to model choice or distributional assumption and was primarily challenged by the complexity of the neural structure of interest.

Researchers like those at USC [14] can use connectivity maps like the ones developed here (Figures 6-11) to better understand the brain and to engineer neural prostheses. However, such inferential maps also come with limitations that must be considered. This analysis operated under the assumption that output neurons with highly predictive models are extensively connected with nearby neurons. While this may imply a high degree of local neural connectivity, it may also imply that only a small output signal was available to model against and so MSE values were necessarily small (e.g., CA1.11). Some influence from lagged values may also be explained by largely inactive output neurons (e.g., CA1.4). Test NMSE values were calculated to alleviate the influence of these limitations but should have been used for all optimization calculations as well. This analysis was further potentially muddled by the resolution of the sensors used in data collection and of the bin size used in modeling. The electrodes used to measure action potentials detect signals from multiple neurons and though a spike-sorting approach was applied to distinguish source neurons, a degree of contamination may remain [15]. Additionally, a bin size of 500 ms was used to discretize the spike train data compared with the 2 ms used by the USC researchers [14]. This decision was made for the sake of signal size and computational complexity but also traded predictive precision in terms of small-scale neural effects for medium-scale insight. These considerations must be examined in future analyses building off the groundwork laid here.

Future research in this area could take many directions moving forward. Certainly, other model frameworks could be explored to increase sensitivity including a generalized autoregressive moving average (GARMA) model [8], a Volterra-Kernel model [15], and a Bayesian model estimated by integrated nested Laplace approximations (INLA) [5]. Additionally, dimension reduction techniques like factor analysis could be applied both exploratorily to identify important input neurons and predictively to improve model accuracy and account for the influence of unrecorded neurons. Finally, efforts could be made to emulate the USC researchers [14] by associating action potential patterns with specific phases of the rat's task to translate directly between neural signals and physical action and habit formation. Advanced neural inference techniques will assuredly continue to develop and become more widely applicable in future years.

References

1   Action potentials and synapses. (2017). https://qbi.uq.edu.au/brain-basics/brain/brain-physiology/action-potentials-and-synapses.

2   Anomaly.io. (2016). Detecting correlation among multiple time series [Accessed: 4/10/2022]. https://anomaly.io/detect-correlation-time-series/index.html.

3   Chen, Z., & Yang, Y. (2004). Assessing forecast accuracy measures. *Iowa State University*.

4   Davis, R., Dunsmuir, W., & Streett, S. (2001). Modeling time series of counts. *Columbia Statistics*.

5   Davis, R., Fokianos, K., Holan, S., Joe, H., Livsey, J., Lund, R., Pipiras, V., & Ravishanker, N. (2021). Count time series: A methodological review. *Journal of the American Statistical Association*.

6   Dunsmuir, W. T. M., & Scott, D. J. (2015). The glarma package for observation-driven time series regression of counts. *Journal of Statistical Software*.

7   How to measure brain activity in people. (2018). *Queensland Brain Institute*. https://qbi.uq.edu.au/brain/brain-functions/how-measure-brain-activity-people.

8   Liboschik, T., Fokianos, K., & Fried, R. (2017). Tscount: An R package for analysis of count time series following generalized linear models. *Journal of Statistical Software*.

9   McCullagh, P., & Nelder, J. A. (1989). *Generalized linear models (2nd ed.)* Chapman and Hall.

10 Research computing user guide. (n.d.). *University of Colorado Boulder*. https://curc.readthedocs.io/en/latest/index.html.

11 Rey, H. G., Pedreira, C., & Quiroga, R. Q. (2015). Past, present and future of spike sorting techniques. *Brain Research Bulletin*.

12 Salles, R., Assis, L., Guedes, G., Bezerra, E., Porto, F., & Ogasawara, E. (2022). A framework for benchmarking machine learning methods using linear models for univariate time series prediction. *Journal of Statistical Software*.

13 Shrivastava, S. (2020). Cross validation in time series [Accessed: 4/10/22]. *Medium*. https://medium.com/@soumyachess1496/cross-validation-in-time-series-566ae4981ce4.

14 Song, D., Harway, M., Marmarelis, V. Z., Hampson, R. E., Deadwyler, S. A., & Berger, T. W. (2014). Extraction and restoration of hippocampal spatial memories with non-linear dynamical modeling. *Frontiers in Systems Neuroscience*.

15 Stanton, G. (2022). Neural data and models [Presentation].

16 Trapletti, A., & Hornik, K. (2022). Tseries: Time series analysis and computational finance. *Journal of Statistical Software*.
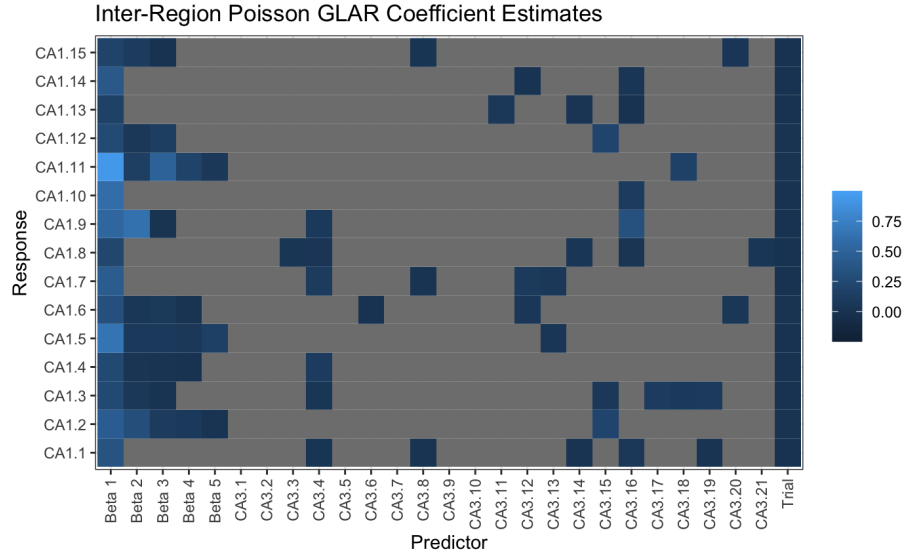
6 Appendix (Coefficient Estimates)

Figure 6: Coefficient estimates from inter-region Poisson GLAR models.
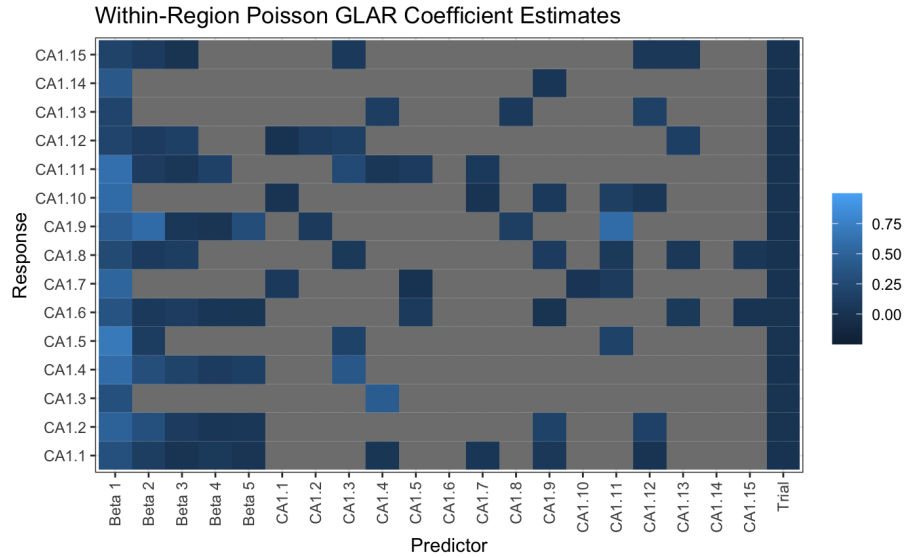

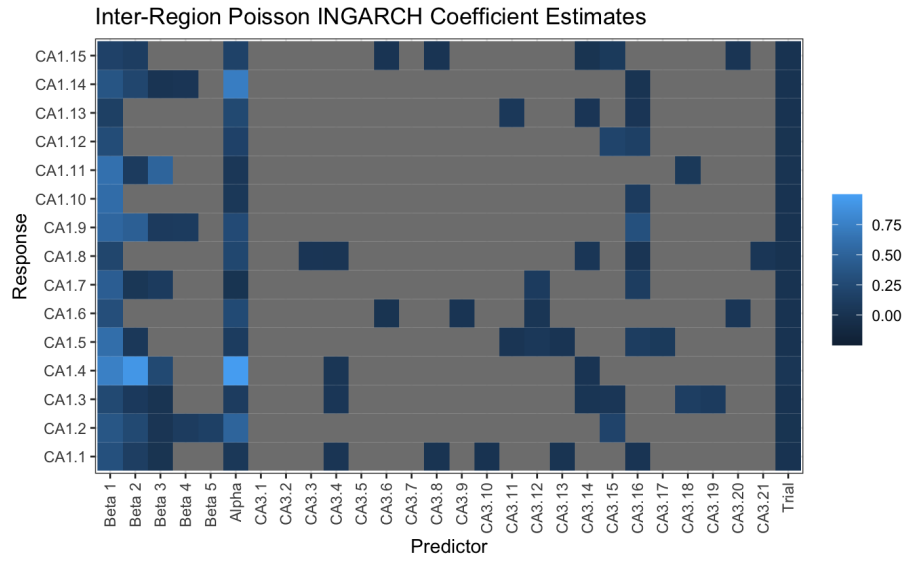Figure 7: Coefficient estimates from within-region Poisson GLAR models.

Figure 8: Coefficient estimates from inter-region Poisson INGARCH models.
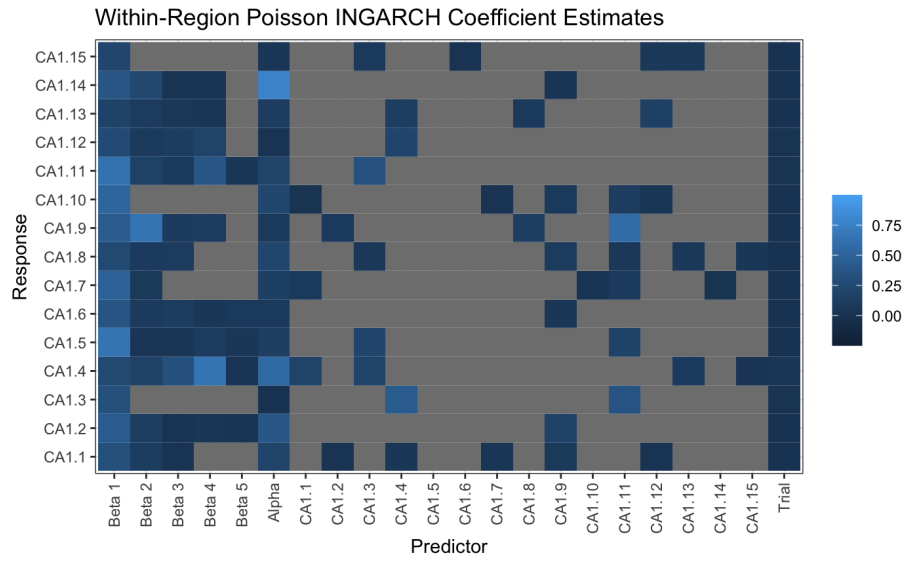

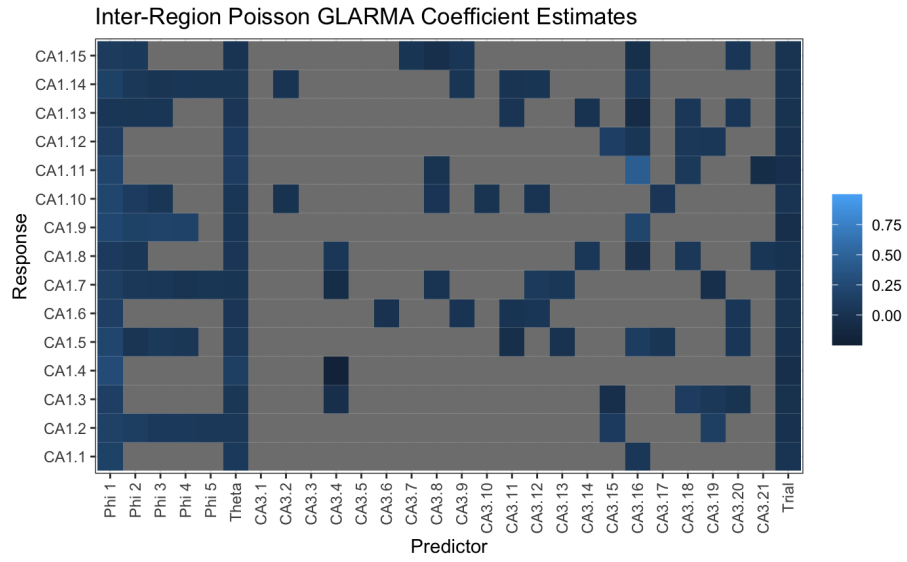Figure 9: Coefficient estimates from within-region Poisson INGARCH models.

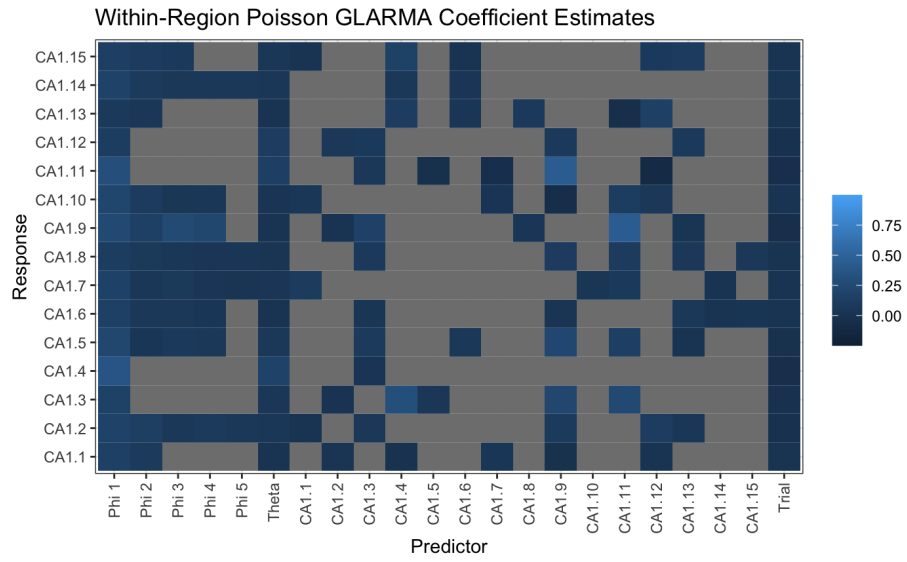Figure 10: Coefficient estimates from inter-region Poisson GLARMA models.

Figure 11: Coefficient estimates from within-region Poisson GLARMA models.